Triple-action self-healing protective coatings based on shape memory polymers containing dual-function microspheres

Huang, Yao; Deng, Leping; Ju, Pengfei; Huang, Luyao; Qian, Hongchang; Zhang, Dawei; Li, Xiaogang; Terryn, Herman A.; Mol, Johannes M.C.

DOI
10.1021/acsami.8b06985

Publication date
2018

Document Version
Final published version

Published in
ACS Applied Materials and Interfaces

ACS APPLIED MATERIALS & INTERFACES

Research Article

Cite This: ACS Appl. Mater. Interfaces 2018, 10, 23369−23379

www.acsami.org

Triple-Action Self-Healing Protective Coatings Based on Shape Memory Polymers Containing Dual-Function Microspheres

Yao Huang,[†,⊥] Leping Deng,[†,⊥] Pengfei Ju,[‡] Luyao Huang,[†] Hongchang Qian,[†] Dawei Zhang,*[,†] Xiaogang Li,[†] Herman A. Terryn,[§] and Johannes M. C. Mol[∥]

[†]Corrosion and Protection Center, Institute for Advanced Materials and Technology, University of Science and Technology Beijing, Beijing 100083, China

[‡]Shanghai Aerospace Equipment Manufacturer, Shanghai 200245, China

[§]Department of Materials and Chemistry, Research Group Electrochemical and Surface Engineering, Vrije Universiteit Brussel, Brussels 1050, Belgium

[∥]Department of Materials Science and Engineering, Delft University of Technology, Delft 2628, The Netherlands

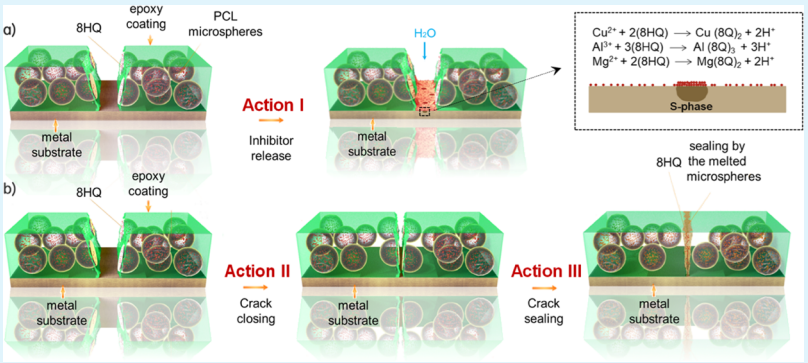

ABSTRACT: In this study, a new self-healing shape memory polymer (SMP) coating was prepared to protect the aluminum alloy 2024-T3 from corrosion by the incorporation of dual-function microspheres containing polycaprolactone and the corrosion inhibitor 8-hydroxyquinoline (8HQ). The self-healing properties of the coatings were investigated via scanning electron microscopy, electrochemical impedance spectroscopy, and scanning electrochemical microscopy following the application of different healing conditions. The results demonstrated that the coating possessed a triple-action self-healing ability enabled by the cooperation of the 8HQ inhibitor, the SMP coating matrix, and the melted microspheres. The coating released 8HQ in a pH-dependent fashion and immediately suppressed corrosion within the coating scratch. After heat treatment, the scratched coating exhibited excellent recovery of its anticorrosion performance, which was attributed to the simultaneous initiation of scratch closure by the shape memory effect of the coating matrix, sealing of the scratch by the melted microspheres, and the synergistic effect of corrosion inhibition by 8HQ.

KEYWORDS: *corrosion, self-healing coating, corrosion inhibitor, shape memory polymer, smart materials*

1. INTRODUCTION

As the most widely used method to mitigate corrosion, polymer coatings provide physical barriers against corrosive media and suppress cathodic and anodic reactions on the underlying metallic substrates.[1] However, the coatings are susceptible to damage caused by mechanical or environmental attack during construction, transportation, and service and require costly and labor-intensive reparation or replacement. In this sense, the development of smart coatings that can repair the damage themselves or with minimal external intervention has received considerable interest in the last decade.[2−7]

For corrosion protection, the most common self-healing strategy is to embed corrosion inhibitors as active healing agents in the coating matrix.[8−17] These corrosion inhibitors can leach into the coating defect and immediately suppress the corrosion reactions that take place at the exposed metal substrate. In many cases, proper encapsulation of the inhibitor is beneficial to preserve its reactivity and to achieve its sustained and environmentally (pH-, Cl-, redox) responsive delivery within the coating defect.[18−24] The containers for encapsulating corrosion inhibitors can be inorganic nanoparticles made of layered double hydroxides,[25,26] halloysites,[27,28] and mesoporous SiO_2,[21,24] or organic micro- or nanocapsules, such as polyelectrolyte microcapsules,[29,30] fibers,[31] and hollow polymeric microspheres.[32,33] For inhibitor-based coatings, the healing effects result from corrosion

Received: April 28, 2018
Accepted: June 21, 2018
Published: June 21, 2018

DOI: 10.1021/acsami.8b06985
ACS Appl. Mater. Interfaces 2018, 10, 23369−23379

Scheme 1. Triple-Action Self-Healing Mechanism Enabled by (a) 8HQ Released From PCL Microspheres to Inhibit Localized Corrosion Mainly by the S-Phase Intermetallics Composed of Al_2CuMg (Action I), (b) Synergistic Effect of Crack Closing by the Shape Memory Epoxy Polymer (Action II) and Crack Sealing by the Melted Microspheres (Action III)

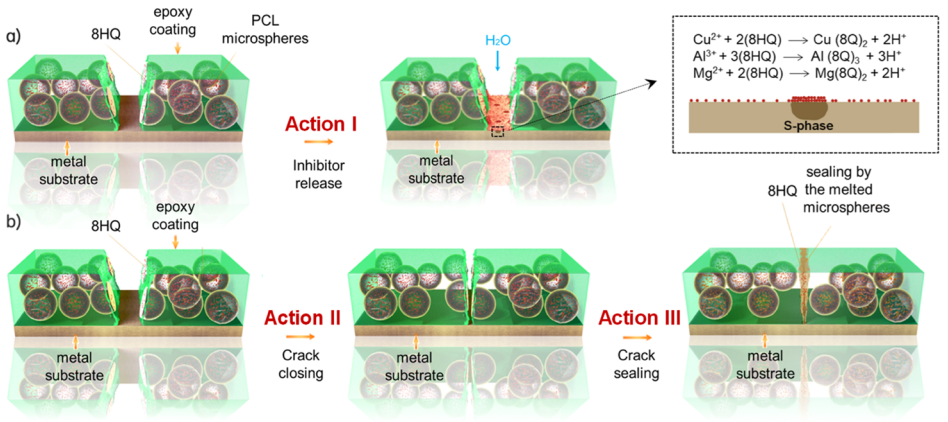

inhibition rather than by intrinsic repair of the barrier properties of the coating. Therefore, the healing efficiency depends critically on the intrinsic performance, irreversibility, leaching capacity, and the amount of inhibitor in the coating. At low-leached inhibitor levels, the effective suppression of corrosion by the corrosion inhibitor in large coating defects is difficult to achieve. However, with larger amounts of the inhibitor, the barrier properties of the coatings may be reduced, as more diffusion channels are created at the container−coating interfaces.[3]

Besides, through the active corrosion inhibition, the corrosion protection of the coating can also be restored based on coating matrix mobility, which is most often initiated by an external stimulus of heat or light.[34−38] For instance, thermoresponsive shape memory polymers (SMPs) have been used to prepare self-healing coatings whose bulk integrity and surface morphology can be recovered after temporary deformation.[39−41] Some of the early systems of this type used polyurethane SMPs containing soft poly(ε-caprolactone) (PCL) segments as the coating material. Heating above the melting transition temperature (T_m) of PCL softened the PCL segments and triggered the shape memory effect. As a result, damage to the coating, such as mechanical scratches, could be physically closed to partially restore the barrier properties of the coating, although an unbonded crevice remained at the damage site. For SMP-based coatings, the self-healing effect can be initiated by artificial heating or the heat generated by (sun)light irradiation.[38] This thermally initiated self-healing process may also be facilitated by a complementary corrosion sensing component in the coating, which can locate the coating damage, enabling a more timely and efficient repair.[42,43]

To further enhance the healing efficiency, a dual-action "close-then-heal" strategy was demonstrated by incorporating thermoplastic fillers in SMPs.[44] For example, Mather et al. infused an epoxy SMP into an electrospun PCL fiber scaffold applied on a steel substrate.[35] Increasing the temperature to 80 °C simultaneously triggered the shape memory effect to close the scratch and the melting of PCL fibers to rebond the scratch side walls. A different concept for dual-action self-healing coatings can be realized in SMP coatings by the incorporation of corrosion inhibitors. Recently, we directly doped benzotriazole (BTA) in an epoxy SMP coating applied on carbon steel. In the absence of heating, the BTA that leached at the coating scratch initiated the immediate inhibition of corrosion. In return, the SMP improved the inhibitory efficiency of BTA by remarkably reducing the size of the damaged area.[45]

In this work, we report on the development of a novel triple-action self-healing SMP coating containing dual-function PCL microspheres for the protection of the aluminum alloy 2024-T3 (AA2024-T3) from corrosion. As shown in Scheme 1a, on the one hand, the microspheres served as carriers of the corrosion inhibitor 8-hydroxyquinoline (8HQ), which leached from the microspheres and suppressed corrosion when the coating was damaged. On the other hand (Scheme 1b), when heat was applied, the shape memory effect induced the closure of the coating scratch, which was further sealed by the simultaneous melting of the inhibitor-loaded microspheres. As such, the triple-action self-healing mechanism of this coating concept involves (i) inhibitor release, (ii) scratch closure, and (iii) scratch sealing for robust corrosion protection restoration at coating defects. The damaged and healed morphologies of the coatings were observed using scanning electron microscopy (SEM). Triple-action self-healing mechanisms and the healing efficiency were investigated via electrochemical impedance spectroscopy (EIS) and scanning electrochemical microscopy (SECM) following the application of different healing conditions.

2. EXPERIMENTAL SECTION

2.1. Materials. PCL (molecular weight: ~45 000 g/mol), bisphenol A diglycidyl ether (BADGE), and Jeffamine D230 hardener were purchased from Sigma-Aldrich. Polyvinyl alcohol (PVA) (molecular weight: ~27 000 g/mol), *n*-decylamine, and 8HQ were supplied by Shandong Xiya Chemical Industry, Co. Ltd. All chemicals and solvents were used as received.

2.2. Preparation of Microspheres. 8HQ-loaded microspheres were prepared using an oil-in-water (O/W) emulsion solvent evaporation method. The typical preparation procedures are as follows: A solution containing 0.3 g PCL and 0.2 g 8HQ in 20 mL dichloromethane was added to 100 mL of a PVA aqueous solution (0.15 w/v %) and homogenized under sonication (FLUKO F6/10) for 5 min with a stirring speed of 15 000 rpm. The resulting O/W emulsion was magnetically stirred at a speed of 80 rpm for 2.5 h until the solvent completely evaporated. The obtained microspheres were centrifuged, washed in deionized water two times, and finally freeze-dried for 24 h. As a control, inhibitor-free pure PCL microspheres were also prepared using a similar method.

2.3. Characterization of Microspheres. The morphology and size of the microspheres were analyzed using SEM (FEI Quanta 250) at an accelerating voltage of 20 kV. Prior to SEM observation, the

DOI: 10.1021/acsami.8b06985
ACS Appl. Mater. Interfaces 2018, 10, 23369−23379

samples were sputtered with gold under an argon atmosphere to improve conductivity.

The amount of 8HQ contained in the PCL microspheres was determined by dissolving the inhibitor-loaded microspheres in dichloromethane. The obtained solution was analyzed using UV spectrophotometry (Hitachi U-3900H). The concentration of 8HQ in dichloromethane was obtained by measuring the absorbance peak from 190 to 450 nm of dichloromethane solutions with a series of 8HQ concentrations. A standard curve of the absorption as a function of the concentration was plotted based on the maximum absorption at 239 nm. The inhibitor loading content [ILC (%)] was calculated using eq 1

$$\text{ILC}\ (\%) = \left(\frac{\text{weight of inhibitor in microsphere}}{\text{weight of microsphere}}\right) \times 100\% \quad (1)$$

2.4. Coating Preparation. AA2024-T3 (80 mm × 60 mm × 5 mm) was used as the coating substrate. Prior to the application of the coating, the substrate was abraded with 240 grit abrasive paper, cleaned with ethanol, and degreased with acetone in an ultrasound bath for 10 min. To prepare the self-healing coating, BADGE, Jeffamine D230, and *n*-decylamine were mixed at a molar ratio of 8:1:6, which was determined based on a previous study,[46] and different amounts (5, 10, and 15 wt %) of pure PCL microspheres were added under mild stirring. The mixture was spread over the aluminum alloy substrate using a rod applicator and cured at 50 °C for 24 h. As a control, a blank SMP coating without PCL microspheres was also similarly prepared. Using the same method, a coating that contained 8HQ-loaded microspheres was prepared at the optimum microsphere concentration, which was determined using self-healing tests performed with SEM analysis and EIS measurements. The thickness of the dry coatings was ∼100 μm.

2.5. Self-Healing Tests. To study the self-healing ability of the coatings, a through-coating scratch was made on the coating surface with a sharp razor blade. The damaged coating was heated in an oven at 80 °C for 30 min to complete the shape memory process of the epoxy coating and to melt the microspheres. The morphology before and after healing was observed using SEM (FEI Quanta 250) under a 10 kV accelerating voltage. To observe the sealing of the scratch by the melted microspheres, the cross section of the coated panel was milled using a focused ion beam (FIB, TESCAN LYRA 3) accelerated at 15 keV upon tilting the sample ±50° from the normal and upon rotation.

To study the release of 8HQ, a free film was prepared by curing the same coating resin (10 wt % 8HQ−PCL microspheres) in a silicone mold at 50 °C for 24 h. The film was then peeled off from the mold and cut into two pieces to expose the full cross section (2.5 × 0.2 cm^2). The cross section of the film was then dipped into a NaCl solution at pH 4, 7, and 10 (tuned by adding HCl or NaOH) for up to 200 h. The amount of 8HQ released into the solution was evaluated using UV spectrophotometry. Standard curves were plotted by measuring a series of 8HQ concentrations dissolved in the NaCl solution.

Elemental analysis was performed by energy-dispersive X-ray spectroscopy (EDS) mapping (ZEISS SUPRA 55) over an area of 2 × 1.6 μm^2 on the exposed aluminum alloy substrate within the coating scratch. The scratched region of the coating was also investigated by infrared spectroscopy (NEXUS 670) in the range of 2000−750 cm^{-1}, with a spot size of 10 × 20 μm^2.

EIS was performed on the scratched and healed coatings immersed in a 3.5 wt % NaCl solution at room temperature using a PARSTAT 2273 electrochemical station. A three-electrode system was used, in which the coated panel functioned as the working electrode, a platinum foil was utilized as the counter electrode, and a saturated calomel electrode (SCE) served as the reference electrode. The area of the working electrode was 3.14 cm^2. The measurements were conducted at the open-circuit potential in the frequency range of 10^5 to 10^{-2} Hz with a 20 mV perturbation. A Faraday cage was used to protect the electrochemical cell from external electromagnetic fields and interference by stray current. Two specimens for each condition were tested to confirm the repeatability.

SECM (Ametek M370) was carried out to monitor oxygen reduction in the scratched regions of coatings containing different microspheres before and after healing. The coating specimens were immersed in a 3.5 wt % NaCl solution for two days during the experiment. A four-electrode electrochemical cell with SCE as the reference electrode, a platinum electrode as the counter electrode, a platinum microelectrode as the probe, and the sample as the working electrode was designed. The distance between the sample and the tip of the platinum microelectrode was maintained at 25 μm during the measurement. A tip potential of −0.75 V (vs SCE) was applied to the platinum tip to operate the SECM in the redox competition mode. The scanned area was 800 × 1000 μm^2, and a scanning rate of 50 μm s^{-1} was utilized. Two specimens for each condition were measured to confirm the repeatability. The oxygen reduction current (i) obtained in the scratch region was normalized by the current obtained over the intact surface where the oxygen is controlled by the steady-state diffusion (i_∞). The values of i/i_∞ were obtained along the center line of the scratch (where oxygen reduction current is the lowest) and their average was used to indicate the healing efficiency.

3. RESULTS AND DISCUSSION

3.1. Encapsulation and Release of the Corrosion Inhibitor. PCL is a biodegradable polyester that has been widely used to prepare controlled release drug carriers in pharmaceutical applications.[47] In this study, PCL microspheres containing the 8HQ corrosion inhibitor were successfully prepared using an O/W emulsion solvent evaporation technique.[48] According to previous studies, the method was expected to produce a homogeneous distribution of the hydrophobic 8HQ inhibitor within the hydrophobic PCL microspheres.[49,50] Dichloromethane was chosen as the organic phase of the O/W emulsion because of its low boiling point (40 °C), which is beneficial for the solidification of the microspheres. The size of the microspheres decreased with increased stirring speed and with increasing stirring time. Figure 1a,b shows SEM images of the pure PCL and 8HQ-loaded microspheres, respectively. The microspheres possess a spherical shape and have an average diameter of ∼4 μm. The incorporation of 8HQ in the PCL microspheres did not significantly impact the microsphere size or morphology.

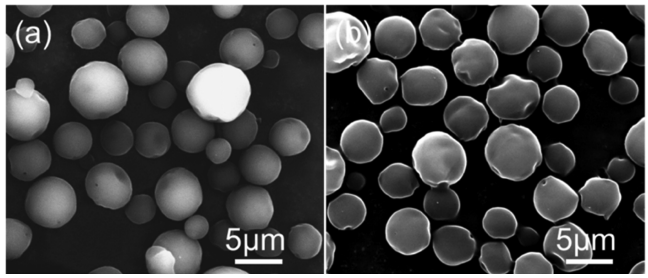

Figure 1. SEM images of microspheres: (a) pure PCL microspheres and (b) 8HQ−PCL microspheres.

The encapsulation of 8HQ in the microspheres was quantitatively analyzed by performing UV spectrophotometry on 8HQ-doped microspheres dissolved in dichloromethane. To calculate the ILC(%), the absorption at 239 nm in the UV spectrum was measured and compared with the standard curves of 8HQ dissolved in dichloromethane.[51] The result revealed an ILC(%) value of ∼21%, which was relatively high compared to that of other common organic containers for corrosion inhibitors in self-healing coatings.[52−54] To simulate

DOI: 10.1021/acsami.8b06985
ACS Appl. Mater. Interfaces 2018, 10, 23369−23379

the conditions of inhibitor release during the self-healing events, the 8HQ release profiles were determined from the fresh cross section of the coating containing 8HQ–PCL microspheres rather than from free microspheres. As shown in Figure 2, PCL microspheres were clearly able to more rapidly

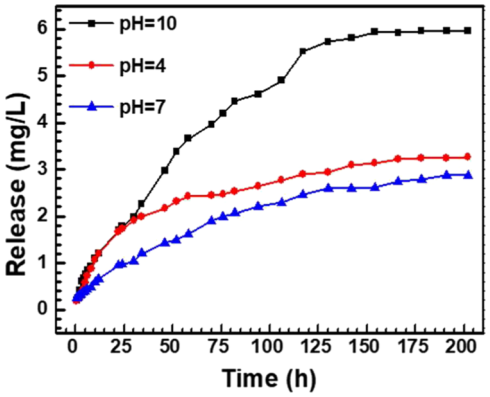

Figure 2. Cumulative amount of 8HQ released with time in NaCl solutions of different pH.

release the encapsulated 8HQ at pH = 10 than at other pH values. The degradation of PCL microspheres was faster under alkaline conditions because of the autocatalytic decomposition of the ester bonds.[55] All of the release curves exhibited a faster release rate within the first 24 h as compared to later stages of exposure, which is considered an advantage for corrosion protection, as the rapid leaching of inhibitors ensures immediate suppression of corrosion reactions when the coating is damaged.[56]

3.2. Differential Scanning Calorimetry (DSC) Study. In this study, the scratched surface of the coating was healed by heating the sample above the glass transition temperature (T_g) of the epoxy SMP and the T_m of the microspheres. The DSC curves (Figure 3) reveal that the T_g of the blank SMP coating

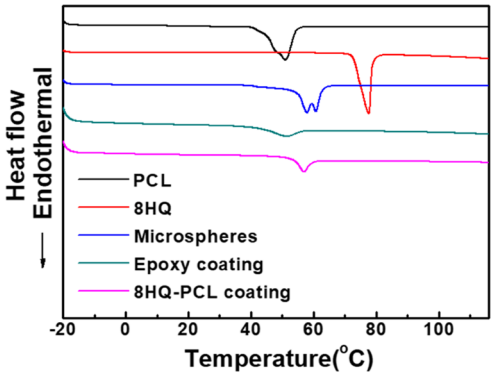

Figure 3. DSC curves of PCL, 8HQ, microspheres, and coatings.

is ~46 °C. The DSC curves of pure PCL microspheres and free 8HQ inhibitor present sharp endothermic peaks at ~50 and ~78 °C, respectively, which correspond to their melting points. For the 8HQ–PCL microspheres, the endothermic peaks are located between those of PCL and 8HQ, indicating a certain miscibility between the components of the microspheres.[57] For the coatings containing 8HQ–PCL microspheres, the addition of microspheres hindered the segmental mobility of the epoxy, which led to a slight increase in T_g.[58] As a result, the T_g of the epoxy and the T_m of the microspheres overlap, showing only one peak at ~57 °C in the corresponding DSC curve. On the basis of these results, the scratched coatings were heated at 80 °C for 30 min to study their self-healing behaviors. Under these heating conditions, the shape memory effect is expected to be triggered, and both PCL and 8HQ are expected to melt and flow into the coating scratch.

3.3. Effect of the Microsphere Amount. To identify the optimal amount of microspheres, the thermally induced self-healing behaviors of coatings that contained 0, 5, 10, and 15 wt % PCL microspheres were tested and compared. Figure 4

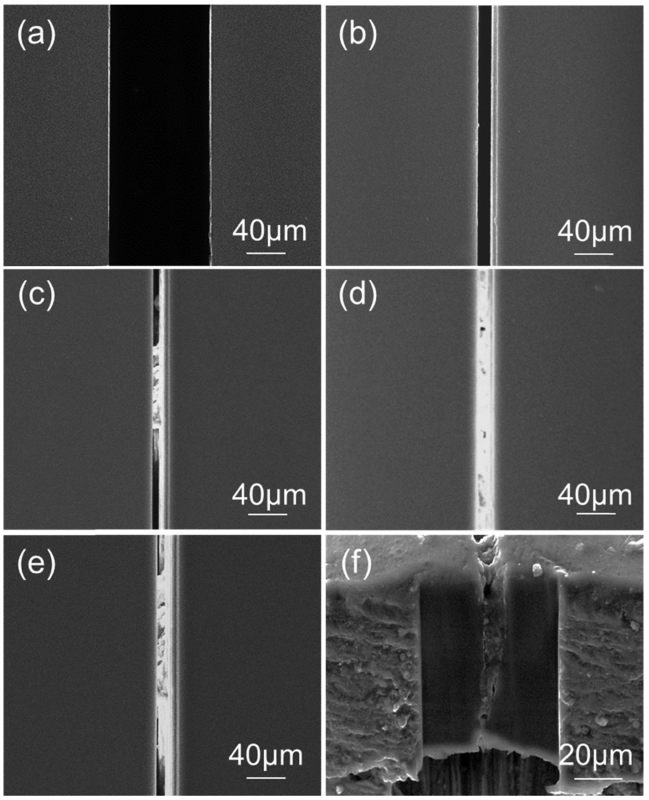

Figure 4. SEM images of the self-healing coating surfaces: (a) originally scratched surface, (b) heated blank SMP coating, (c) heated coating with 5 wt % PCL microspheres, (d) heated coating with 10 wt % PCL microspheres, (e) heated coating with 15 wt % PCL microspheres, and (f) FIB-prepared cross section of the healed scratch area of the coating with 10 wt % PCL microspheres.

shows representative surface morphologies of the scratched and thermally repaired coatings. The initial width of the through-coating scratches was ~100 μm (Figure 4a). After heating, the scratches in all the coatings shrank to a width of only ~15 μm, suggesting that the presence of PCL microspheres did not affect the shape memory ability of the epoxy coating. Compared to the blank SMP coating shown in Figure 4b, for the coatings containing PCL microspheres, the remaining gaps observed in Figure 4c–e were partially or fully filled after heating. In addition, a larger extent of filling was observed when the amount of PCL microspheres reached 10–15 wt %. An FIB was used to prepare a cross section of the scratched region of the healed coatings. For the coating with 10 wt % PCL microspheres (Figure 4f), the representative SEM image shows that the melted microspheres completely

DOI: 10.1021/acsami.8b06985
ACS Appl. Mater. Interfaces 2018, 10, 23369–23379

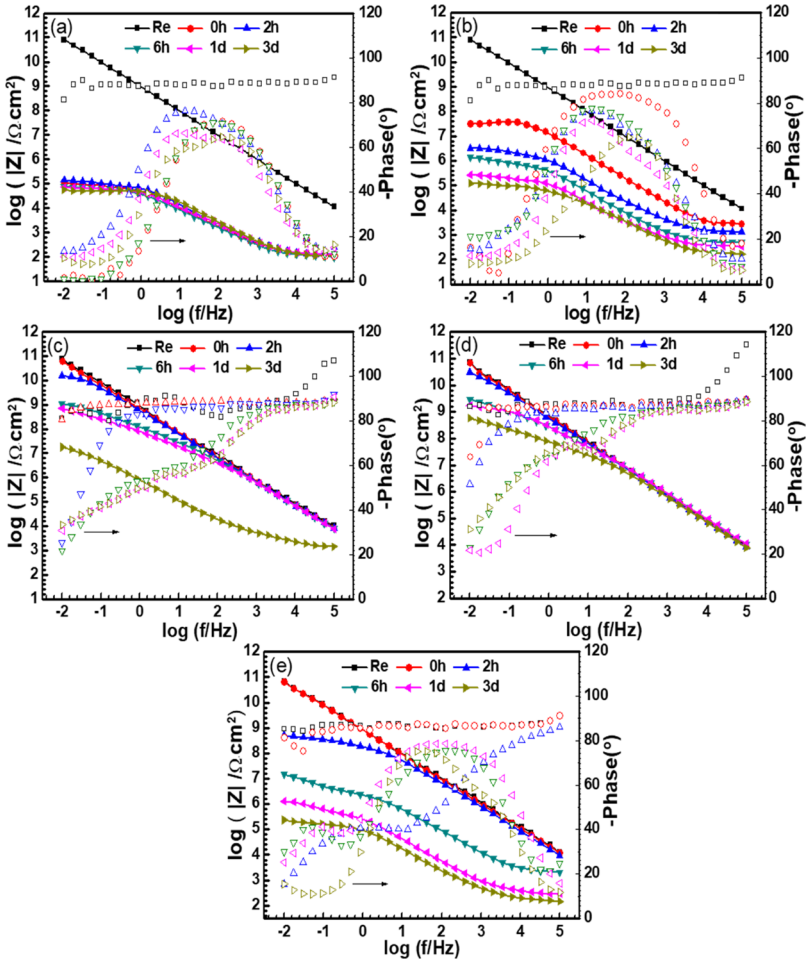

Figure 5. Evolution of Bode plots of the scratched coatings immersed in 3.5 wt % NaCl solution for 3 days: (a) blank SMP coating before heating, (b) heated blank SMP coating, (c) heated coating with 5 wt % PCL microspheres, (d) heated coating with 10 wt % PCL microspheres, and (e) heated coating with 15 wt % PCL microspheres. The closed symbols represent impedance modulus values, and the open symbols indicate phase angles.

filled the remaining gap of the closed scratch and repaired the physical barrier of the coating.

The effect of the microsphere quantity on the self-healing performance was further investigated by comparing the barrier properties of the healed coatings based on EIS measurements in a 3.5 wt % NaCl solution. To rule out the effect of the simultaneously increased 8HQ quantity, pure PCL microspheres instead of 8HQ−PCL microspheres were incorporated in the coatings. Figure 5 shows EIS results as Bode plots for coatings containing different amounts of pure PCL microspheres after 0, 2, and 6 h and 1 and 3 d of immersion. The impedance modulus at 0.01 Hz ($|Z|_{0.01Hz}$) of Bode plots has often been used as a semi-quantitative indicator for the anticorrosion performance of coatings. The Bode plot of the intact coating demonstrated a pure capacitive behavior, with $|Z|_{0.01Hz}$ reaching to $\sim 10^{11}$ Ω cm^2. The corresponding phase angles remain at approximately −90° over the entire frequency range, indicating a near-ideal barrier performance of the intact coating. From comparison of the $|Z|_{0.01Hz}$ values of blank SMP coatings before (Figure 5a) and after (Figure 5b) heating, the shape memory effect clearly partially recovers the barrier effect of the coating based on the reduced scratch size. However, this self-healing effect quickly diminished during immersion because water was able to penetrate the unbonded crevice of the closed scratch. As shown in Figure 5b, the $|Z|_{0.01Hz}$ value decreased from 3.1×10^7 to 1.2×10^5 Ω cm^2 after 3 days of immersion when the barrier property was completely lost. This finding was in good agreement with those previously reported for self-healing coatings based on pure SMPs.[37,59] In phase diagrams, the broad time constant in the medium-frequency range can be ascribed to two combined time constants, including the pore resistance of the coating and the oxide layer on the exposed metal substrate (typically in the range of 1−0.1 Hz). The time constant in the low-frequency region typically reflects corrosion activities such as pitting on the exposed substrate,[60,61] which became slightly visible after 3 days of immersion, as shown in Figure 5a. In comparison, a broader time constant in the medium-frequency range shown in Figure 5b was observed at the beginning of the immersion because of the reduced scratch size.

In contrast to the blank coating, coatings containing 5, 10, and 15 wt % microspheres exhibited a repaired barrier effect after heating at 80 °C for 30 min. At the beginning of immersion, Bode plots of all of the coatings exhibited 45° straight lines, with $|Z|_{0.01Hz}$ values beyond 5×10^{10} Ω cm^2 (Figure 5c−e), and the corresponding phase angles were −90° over the entire frequency range. Clearly, this full recovery of barrier properties of the coating was attributed to not only the closure of the scratch by the shape memory effect but also the sealing of the remaining gaps by the melted microspheres. As

DOI: 10.1021/acsami.8b06985
ACS Appl. Mater. Interfaces 2018, 10, 23369−23379

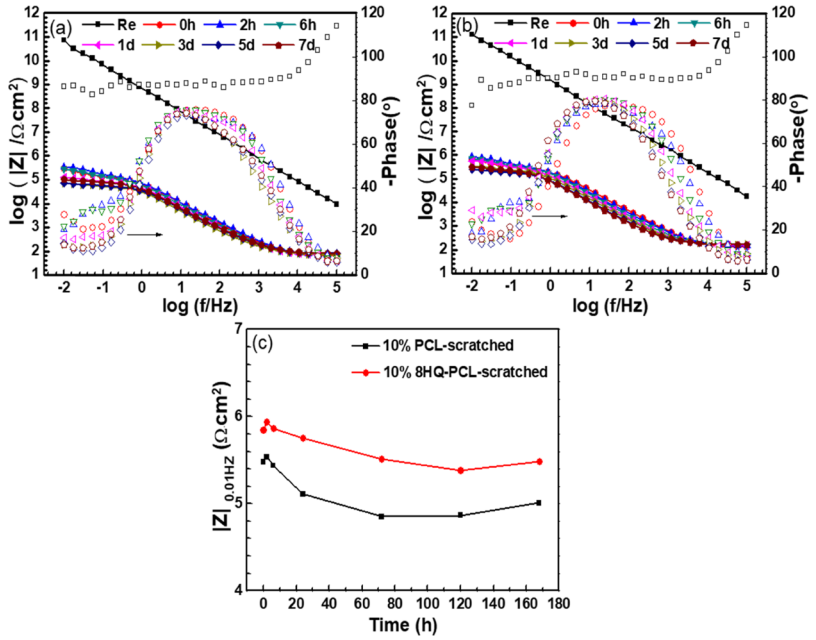

Figure 6. Bode plots of (a) scratched coatings with 10 wt % PCL microspheres and (b) scratched coatings with 10 wt % 8HQ−PCL microspheres after 0, 2, and 6 h and 1, 3, 5, and 7 d of immersion in 3.5 wt % NaCl solution; (c) comparison between $|Z|_{0.01Hz}$ values for scratched coatings with 10 wt % 8HQ−PCL microspheres and 10 wt % PCL microspheres. Closed symbols represent impedance modulus values, and open symbols show phase angles.

immersion continued, the NaCl solution slowly penetrated the repaired scratch, leading to a continuous decrease in the impedance moduli. In phase diagrams, the narrower time constant in the high-frequency region and the increased phase angle in the low-frequency region both revealed the degrading barrier properties of the repaired coatings. After 3 days, $|Z|_{0.01Hz}$ values of the coatings with 5 and 10 wt % PCL microspheres decreased to 1.8×10^7 and 5.8×10^8 Ω cm^2, respectively, which were both significantly higher than that of the blank SMP coating. The coating with 10 wt % microspheres also clearly had a better healing efficiency than the one with 5 wt % microspheres, which agrees well with the morphological observations in Figure 5. With a larger amount of microspheres in the coating, more spheres were exposed at the scratch interface and were therefore available to seal the remaining gaps after melting. However, the coating with 15 wt % PCL microspheres showed an unexpectedly rapid deterioration of the barrier performance (Figure 5e). Despite the high $|Z|_{0.01Hz}$ value observed at the beginning of immersion, the value sharply fell to only 2.3×10^5 Ω cm^2 within 3 days. Correspondingly, the phase angles increased in the high-frequency region. A more defined time constant occurred in the low-frequency range as an indicator of the corrosion activity on the metal substrate. This phenomenon can be explained by the fact that this large amount of microspheres damaged the integrity of the coating matrix by introducing more diffusion channels at the microsphere−coating interfaces.[62] On the basis of the preliminary assessment above, the coating with 10 wt % microspheres was selected as the best composition and used in the following sections, which focused on clarifying the different healing mechanisms in the coatings.

3.4. Self-Healing Mechanism Based on 8HQ. To study the healing effect induced by the corrosion inhibitor, the coating with 10 wt % 8HQ−PCL microspheres was scratched and immersed in 3.5 wt % NaCl solution for EIS measurements, and the results were compared with those for the scratched coating containing pure PCL microspheres. Figure 6 presents variations in the Bode plots for each coating during a 7-day immersion period. Because of the wide openings of the scratches, the $|Z|_{0.01Hz}$ values of both types of coatings were much lower than those of the thermally repaired coatings at the beginning of the tests. Similar phase diagrams were observed, consisting of a broad time constant over the medium frequencies and a weakly defined time constant at the low frequency. For the coating containing pure PCL microspheres, the corrosion reactions occurring within the scratch resulted in a low $|Z|_{0.01Hz}$ value of ~3.0×10^5 Ω cm^2, which continued to decrease over the 7 days of immersion. The coating containing 8HQ−PCL microspheres exhibited a similar variation, but its impedance values were higher than those of the inhibitor-free coating throughout the entire immersion test (Figure 6c). For the coating containing 8HQ, the phase angles in the medium frequencies were slightly higher than those for the inhibitor-free coating, which reflects the improvement of the oxide layer. After 7 days, the $|Z|_{0.01Hz}$ values of the coatings containing pure PCL microspheres and 8HQ−PCL spheres decreased to ~1.0×10^5 and ~3.1×10^5 Ω cm^2, respectively. These results indicate that the presence of 8HQ in the PCL microspheres could improve the corrosion resistance of the coatings after damage occurred.

To confirm that the self-healing effect indeed resulted from the leached 8HQ, scratched regions of coatings containing 8HQ−PCL microspheres and PCL microspheres were further characterized using SEM and EDS analyses. For the coating containing 8HQ−PCL microspheres (Figure 7a), an insoluble film gradually formed in the scratch, which can likely be attributed to complexation between 8HQ and the metallic ions released from the metal substrate. According to the literature, 8HQ can inhibit localized corrosion of AA2024 by forming insoluble complexes over the active sites, such as S-phase (Al_2CuMg) intermetallics.[61,63,64]

DOI: 10.1021/acsami.8b06985
ACS Appl. Mater. Interfaces 2018, 10, 23369−23379

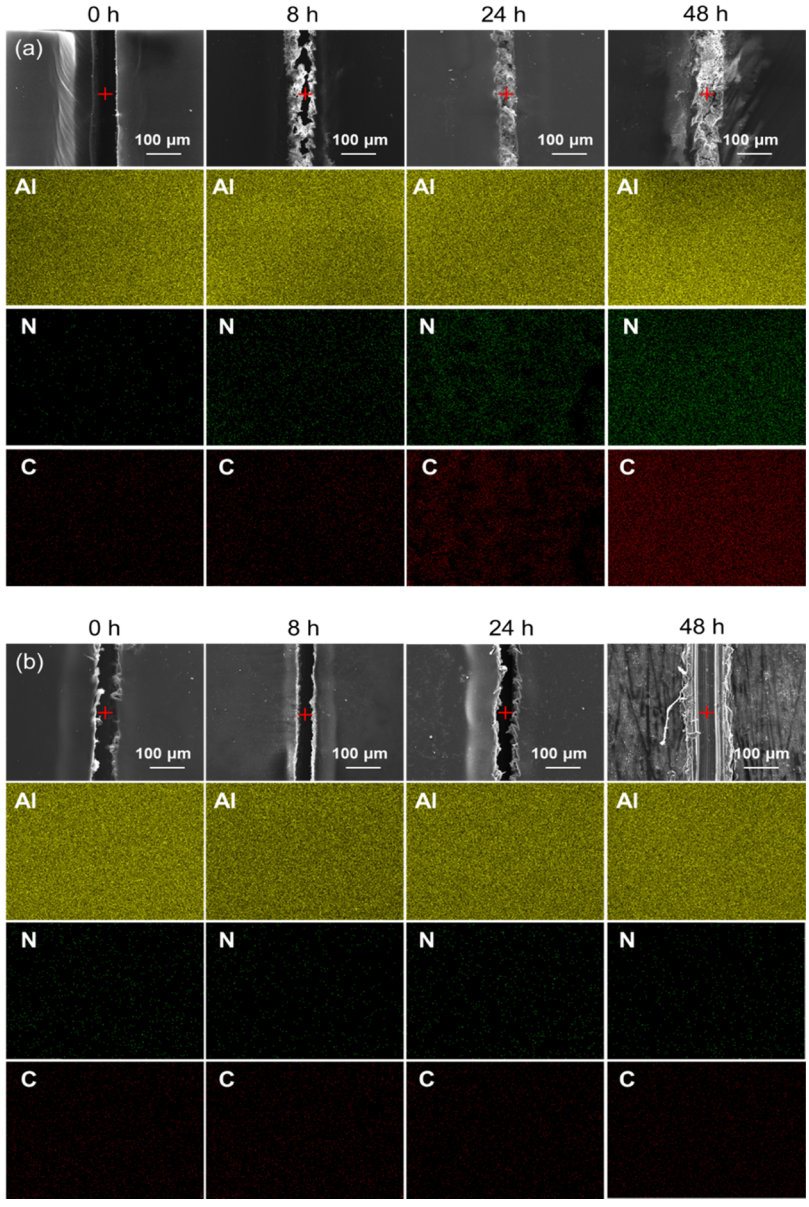

Figure 7. EDS maps in the scratched area of (a) coatings with 10 wt % 8HQ–PCL and (b) 10 wt % PCL microspheres after immersion in 3.5 wt % NaCl for 0, 8, 24, and 48 h. The EDS map was taken over an area of 2 × 1.6 μm^2 at the location indicated by the red cross in the SEM image.

From the EDS measurement, the elemental distribution in the marked area showed a strong signal for Al in the exposed aluminum alloy substrate. The elements N and C became more densely distributed as the immersion time increased, which verifies that the insoluble complex film originated from the 8HQ inhibitor. For the coating containing pure PCL spheres (Figure 7b), however, the scratched region of the coating remained clean during the 48 h of immersion, and minimal N or C was detected.

Figure 8 presents the Fourier transform infrared (FT-IR) spectra recorded on the complex film formed within the scratch of the coating containing 8HQ–PCL microspheres. The bands observed at 1499 and 1463 cm^{-1} in the spectra correspond to aromatic C═C bending vibrations. The bands at 1381 and 1325 cm^{-1} are attributed to the in-plane bending vibrations and deformation vibrations, respectively, of aromatic amines. The peak at approximately 1116 cm^{-1} can be ascribed to stretching vibrations of C–O. The bands at 834 and 768

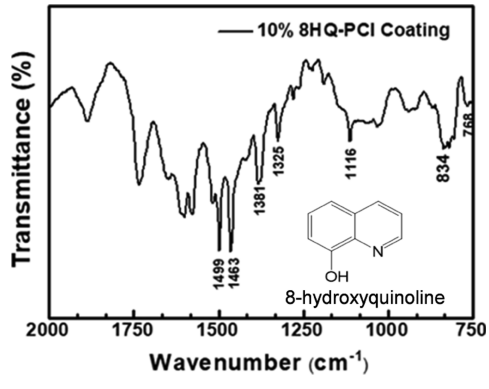

Figure 8. FT-IR spectrum obtained from the scratched coating (containing 10 wt % 8HQ–PCL microspheres) after immersion in 3.5 wt % NaCl solution for 48 h.

DOI: 10.1021/acsami.8b06985
ACS Appl. Mater. Interfaces 2018, 10, 23369–23379

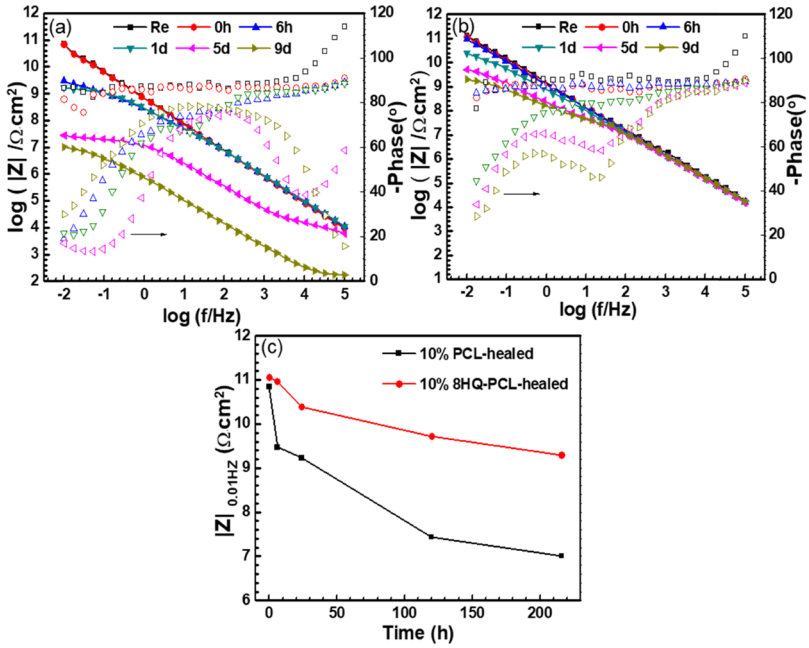

Figure 9. Bode plots of (a) heated coatings with 10 wt % PCL microspheres and (b) heated coatings with 10 wt % 8HQ–PCL microspheres after 0 and 6 h and 1, 5, and 9 d of immersion in 3.5 wt % NaCl solution; (c) comparison between $|Z|_{0.01Hz}$ values for heated coatings with 10 wt % 8HQ–PCL microspheres and 10 wt % PCL microspheres. The closed symbols represent impedance modulus values, and the open symbols indicate phase angles.

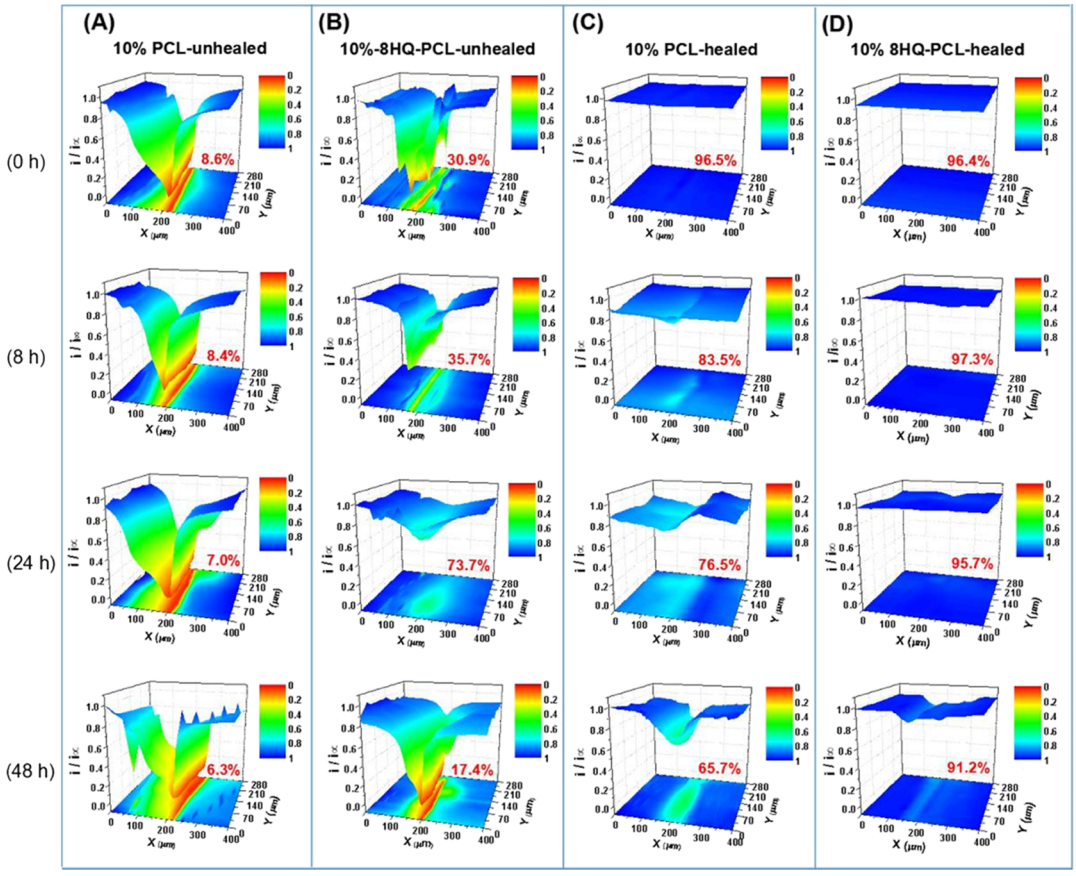

Figure 10. SECM maps of the scratch regions on (a) scratched coatings with 10 wt % PCL microspheres, (b) scratched coatings with 10 wt % 8HQ–PCL microspheres, (c) heated coatings with 10 wt % PCL microspheres, and (d) heated coatings with 10 wt % 8HQ–PCL microspheres after immersion in 3.5 wt % NaCl solution for 0, 8, 24, and 48 h.

DOI: 10.1021/acsami.8b06985
ACS Appl. Mater. Interfaces 2018, 10, 23369–23379

cm^{-1} represent the stretching vibrations of the aromatic C−H bond.[65] Thus, the results of the FT-IR spectra further confirmed the existence of the inhibitor complex.

3.5. Triple-Action Self-Healing Mechanisms. In this section, the coatings containing 10 wt % pure PCL microspheres and 10 wt % 8HQ−PCL microspheres were both scratched and then repaired under heating at 80 °C for 30 min. The healing efficiency of the coatings was first assessed using EIS measurements taken in 3.5 wt % NaCl solution (Figure 9). At the beginning of immersion, both coatings demonstrated excellent restoration of barrier properties with $|Z|_{0.01Hz}$ values higher than 10^{10} Ω cm^2 and pure capacitive behaviors over the whole frequency range, which were attributed to the ability of the coatings to close and fully seal the scratches. For the coating containing pure PCL spheres (Figure 9a), the low-frequency impedance moduli in Bode plots declined slightly within the first day because of the preferential ingress of water through the sealed scratch, which is the most vulnerable point of the coating. After 5 days, more time constants were observed in medium- and low-frequency regions, suggesting that the electrolyte had penetrated the coating most likely through the sealed scratch and corroded the metal substrate underneath. The $|Z|_{0.01Hz}$ value further decreased to ∼1.0×10^7 Ω cm^2 after 9 days of immersion. In comparison, the coating with 10 wt % 8HQ−PCL microspheres showed much slower deterioration of its protective performance, as demonstrated in Figure 9b,c. During the 9 days of immersion, the phase angles at high frequencies remained at −90°. Also, the $|Z|_{0.01Hz}$ value was still well above 10^9 Ω cm^2 after 9 days, which was over two orders of magnitude higher than that of the inhibitor-free coating. This result confirmed that the presence of 8HQ further strengthened the corrosion resistance in the repaired region,[66] thereby prolonging the service life of the repaired coating.

SECM measurements were conducted to provide a more microscopic assessment of the self-healing effects by monitoring oxygen reduction in the scratched region.[45,67] Figure 10 shows the mapping of the oxygen reduction current (i), which is normalized with the steady-state diffusion-controlled current (i_∞). By comparing i/i_∞ obtained over the coating scratches under different healing conditions, the inhibitor-based healing activity and the synergistic effect of SMP and melted microspheres were clearly determined. For the coating containing pure PCL microspheres (Figure 10a), no healing activity was observed in the coating scratch. The oxygen reduction current recorded using the platinum microelectrode at the scratch center remained at nearly zero during the 48 h test, which indicates that the oxygen in this region was almost completely consumed by the cathodic corrosion activity on the exposed substrate.[45,68,69] As shown in Figure 10b, the oxygen reduction reaction in the coating scratch was effectively suppressed within the first 24 h of immersion by the rapidly leached and adsorbed 8HQ inhibitor. As a result, more oxygen was available, and the corresponding oxygen reduction current was higher than that of the inhibitor-free coating, corresponding to a healing efficiency of 73.7%. After 48 h, the oxygen reduction current decreased again, suggesting that the healing effect of the inhibitor was temporary inside the wide-open scratch. After the heat treatment, the physical barrier was well restored in both types of coatings by the closure of the scratch and melting of the microspheres, given that no localized corrosion activity was detected initially (Figure 10c,d). The healing efficiency as reflected by the normalized current reached to ∼96% with or without 8HQ. The current for the coating containing pure PCL microspheres exhibited a small and gradual decrease in the region of the repaired scratch during immersion. For the coating containing 8HQ−PCL microspheres, almost no corrosion activity was observed after 24 h. After 48 h, the current in the scratch region varied only slightly and a healing efficiency over 90% was maintained. Therefore, the coating damage was more effectively repaired by the inhibitor-doped microspheres than by the pure PCL microspheres, demonstrating the durable self-healing performance of the coating.

4. CONCLUSIONS

In this work, a novel SMP-based coating with a triple-action self-healing ability was developed to protect an AA2024-T3 substrate from corrosion upon damage. An improved self-healing performance was achieved by introducing dual-function 8HQ−PCL microspheres, which not only exerted immediate corrosion inhibition in the coating scratch but also melted to fully seal the scratch upon heat treatment. An optimum quantity of 10 wt % microspheres was first determined by assessing the morphology and barrier properties of thermally repaired coatings containing different amounts of PCL microspheres. On the basis of EIS and SECM results, the coating containing 8HQ−PCL microspheres demonstrated triple-action self-healing mechanisms. When the coating was immersed in NaCl solution, the 8HQ inhibitor rapidly leached out of the microspheres and suppressed corrosion within the coating scratch. After heat treatment at 80 °C, the scratch in the coating was closed and sealed by the shape memory effect of the SMP coating matrix in cooperation with the melted microspheres. The physical barrier of the coating was thoroughly restored, and the healing effect was significantly strengthened by the presence of the 8HQ inhibitor in the healed region.

AUTHOR INFORMATION

Corresponding Author

*E-mail: dzhang@ustb.edu.cn.

ORCID

Dawei Zhang: 0000-0002-6546-6181

Johannes M. C. Mol: 0000-0003-1810-5145

Author Contributions

⊥Y.H. and L.D. authors equally contributed to this work.

Notes

The authors declare no competing financial interest.

ACKNOWLEDGMENTS

This work was supported by the National Natural Science Foundation of China (no. 51771029), the Beijing Nova Program (Z171100001117076), the 111 Project (no. B170003), and the National Environmental Corrosion Platform. The authors also acknowledge the helpful discussion with Ali Kosari and Mats Meeusen.

REFERENCES

(1) Hou, B.; Li, X.; Ma, X.; Du, C.; Zhang, D.; Zheng, M.; Xu, W.; Lu, D.; Ma, F. The Cost of Corrosion in China. *npj Mater. Degrad.* **2017**, *1*, DOI: 10.1038/s41529-017-0005-2.

(2) García, S. J.; Fischer, H. R.; van der Zwaag, S. A Critical Appraisal of the Potential of Self Healing Polymeric Coatings. *Prog. Org. Coat.* **2011**, *72*, 211−221.

DOI: 10.1021/acsami.8b06985
ACS Appl. Mater. Interfaces 2018, 10, 23369−23379

(3) Shchukin, D. G. Container-Based Multifunctional Self-Healing Polymer Coatings. *Polym. Chem.* **2013**, *4*, 4871−4877.
(4) Shchukin, D.; Mohwald, H. A Coat of Many Functions. *Science* **2013**, *341*, 1458−1459.
(5) Montemor, M. F. Functional and Smart Coatings for Corrosion Protection: A Review of Recent Advances. *Surf. Coat. Technol.* **2014**, *258*, 17−37.
(6) Wei, H.; Wang, Y.; Guo, J.; Shen, N. Z.; Jiang, D.; Zhang, X.; Yan, X.; Zhu, J.; Wang, Q.; Shao, L.; Lin, H.; Wei, S.; Guo, Z. Advanced Micro/Nanocapsules for Self-Healing Smart Anticorrosion Coatings. *J. Mater. Chem. A* **2015**, *3*, 469−480.
(7) Zhang, D.; Wang, L.; Qian, H.; Li, X. Superhydrophobic Surfaces for Corrosion Protection: A Review of Recent Progresses and Future Directions. *J. Coat. Technol. Res.* **2016**, *13*, 11−29.
(8) Andreeva, D. V.; Fix, D.; Möhwald, H.; Shchukin, D. G. Self-Healing Anticorrosion Coatings Based on pH-Sensitive Polyelectrolyte/Inhibitor Sandwichlike Nanostructures. *Adv. Mater.* **2010**, *20*, 2789−2794.
(9) Mardel, J.; Garcia, S. J.; Corrigan, P. A.; Markley, T.; Hughes, A. E.; Muster, T. H.; Lau, D.; Harvey, T. G.; Glenn, A. M.; White, P. A.; Hardin, S. G.; Luo, C.; Zhou, X.; Thompson, G. E.; Mol, J. M. C. The Characterization and Performance of Ce(dbp)3-Inhibited Epoxy Coatings. *Prog. Org. Coat.* **2011**, *70*, 91−101.
(10) Montemor, M. F.; Snihirova, D. V.; Taryba, M. G.; Lamaka, S. V.; Kartsonakis, I. A.; Balaskas, A. C.; Kordas, G. C.; Tedim, J.; Kuznetsova, A.; Zheludkevich, M. L.; Ferreira, M. G. S. Evaluation of Self-Healing Ability in Protective Coatings Modified with Combinations of Layered Double Hydroxides and Cerium Molibdate Nanocontainers Filled with Corrosion Inhibitors. *Electrochim. Acta* **2012**, *60*, 31−40.
(11) Shi, H.; Han, E.-H.; Lamaka, S. V.; Zheludkevich, M. L.; Liu, F.; Ferreira, M. G. S. Cerium cinnamate as an environmentally benign inhibitor pigment for epoxy coatings on AA 2024-T3. *Prog. Org. Coat.* **2014**, *77*, 765−773.
(12) Mohedano, M.; Blawert, C.; Zheludkevich, M. L. Cerium-Based Sealing of PEO Coated AM50 Magnesium Alloy. *Surf. Coat. Technol.* **2015**, *269*, 145−154.
(13) Liu, Y.; Visser, P.; Zhou, X.; Lyon, S. B.; Hashimoto, T.; Curioni, M.; Gholinia, A.; Thompson, G. E.; Smyth, G.; Gibbon, S. R.; Graham, D.; Mol, J. M. C.; Terryn, H. Protective Film Formation on AA2024-T3 Aluminum Alloy by Leaching of Lithium Carbonate from an Organic Coating. *J. Electrochem. Soc.* **2015**, *163*, 45−53.
(14) Snihirova, D.; Lamaka, S. V.; Taheri, P.; Mol, J. M. C.; Montemor, M. F. Comparison of the Synergistic Effects of Inhibitor Mixtures Tailored for Enhanced Corrosion Protection of Bare and Coated AA2024-T3. *Surf. Coat. Technol.* **2016**, *303*, 342−351.
(15) Visser, P.; Lutz, A.; Mol, J. M. C.; Terryn, H. Study of the Formation of a Protective Layer in a Defect from Lithium-Leaching Organic Coatings. *Prog. Org. Coat.* **2016**, *99*, 80−90.
(16) Mohedano, M.; Serdechnova, M.; Starykevich, M.; Karpushenkov, S.; Bouali, A. C.; Ferreira, M. G. S.; Zheludkevich, M. L. Active Protective PEO Coatings on AA2024: Role of Voltage on In-Situ LDH Growth. *Mater. Des.* **2017**, *120*, 36−46.
(17) Zadeh, M. A.; Tedim, J.; Zhedlukevich, M.; van der Zwaag, S.; Garcia, S. J. Synergetic Active Corrosion Protection of AA2024-T3 by 2D-anionic and 3D-cationic Nanocontainers Loaded with Ce and Mercaptobenzothiazole. *Corros. Sci.* **2018**, *135*, 35−45.
(18) Zheludkevich, M. L.; Shchukin, D. G.; Yasakau, K. A.; Möhwald, H.; Ferreira, M. G. S. Anticorrosion Coatings with Self-Healing Effect Based on Nanocontainers Impregnated with Corrosion Inhibitor. *Chem. Mater.* **2007**, *19*, 402−411.
(19) Plawecka, M.; Snihirova, D.; Martins, B.; Szczepanowicz, K.; Warszynski, P.; Montemor, M. F. Self Healing Ability of Inhibitor-Containing Nanocapsules Loaded in Epoxy Coatings Applied on Aluminium 5083 and Galvanneal Substrates. *Electrochim. Acta* **2014**, *140*, 282−293.
(20) Zheng, Z.; Schenderlein, M.; Huang, X.; Brownbill, N. J.; Blanc, F.; Shchukin, D. Influence of Functionalization of Nanocontainers on Self-Healing Anticorrosive Coatings. *ACS Appl. Mater. Interfaces* **2015**, *7*, 22756−22766.
(21) Ghazi, A.; Ghasemi, E.; Mahdavian, M.; Ramezanzadeh, B.; Rostami, M. The Application of Benzimidazole and Zinc Cations Intercalated Sodium Montmorillonite as Smart Ion Exchange Inhibiting Pigments in the Epoxy Ester Coating. *Corros. Sci.* **2015**, *94*, 207−217.
(22) Ding, C.; Liu, Y.; Wang, M.; Wang, T.; Fu, J. Self-healing, Superhydrophobic Coating Based on Mechanized Silica Nanoparticles for Reliable Protection of Magnesium Alloys. *J. Mater. Chem. A* **2016**, *4*, 8041−8052.
(23) Tavandashti, N. P.; Ghorbani, M.; Shojaei, A.; Gonzalez-Garcia, Y.; Terryn, H.; Mol, J. M. C. pH Responsive Ce(III) Loaded Polyaniline Nanofibers for Self-Healing Corrosion Protection of AA2024-T3. *Prog. Org. Coat.* **2016**, *99*, 197−209.
(24) Ding, C.; Xu, J.; Tong, L.; Gong, G.; Jiang, W.; Fu, J. Design and Fabrication of a Novel Stimulus-Feedback Anticorrosion Coating Featured by Rapid Self-Healing Functionality for the Protection of Magnesium Alloy. *ACS Appl. Mater. Interfaces* **2017**, *9*, 21034−21047.
(25) Galvão, T. L. P.; Neves, C. S.; Zheludkevich, M. L.; Gomes, J. R. B.; Tedim, J.; Ferreira, M. G. S. How Density Functional Theory Surface Energies May Explain the Morphology of Particles, Nanosheets, and Conversion Films Based on Layered Double Hydroxides. *J. Phys. Chem. C* **2017**, *121*, 2211−2220.
(26) Luo, X.; Yuan, S.; Pan, X.; Zhang, C.; Du, S.; Liu, Y. Synthesis and Enhanced Corrosion Protection Performance of Reduced Graphene Oxide Nanosheet/ZnAl-Layered Double Hydroxides Composite Films by Hydrothermal Continuous Flow Method. *ACS Appl. Mater. Interfaces* **2017**, *9*, 18263−18275.
(27) Shchukina, E.; Grigoriev, D.; Sviridova, T.; Shchukin, D. Comparative Study of the Effect of Halloysite Nanocontainers on Autonomic Corrosion Protection of Polyepoxy Coatings on Steel by Salt-Spray Tests. *Prog. Org. Coat.* **2017**, *108*, 84−89.
(28) Shchukina, E.; Shchukin, D.; Grigoriev, D. Effect of Inhibitor-Loaded Halloysites and Mesoporous Silica Nanocontainers on Corrosion Protection of Powder Coatings. *Prog. Org. Coat.* **2016**, *102*, 60−65.
(29) Leal, D. A.; Riegel-Vidotti, I. C.; Ferreira, M. G. S.; Marino, C. E. B. Smart Coating Based on Double Stimuli-Responsive Microcapsules Containing Linseed Oil and Benzotriazole for Active Corrosion Protection. *Corros. Sci.* **2018**, *130*, 56−63.
(30) Beyer, S.; Schürmann, R.; Feldmann, I.; Blocki, A.; Bald, I.; Schneider, R. J.; Emmerling, F. Maintaining Stable Zeolitic Imidazolate Framework (ZIF) Templates during Polyelectrolyte Multilayer Coating. *Colloid Interface Sci. Commun.* **2018**, *22*, 14−17.
(31) Yabuki, A.; Shiraiwa, T.; Fathona, I. W. pH-Controlled Self-Healing Polymer Coatings with Cellulose Nanofibers Providing an Effective Release of Corrosion Inhibitor. *Corros. Sci.* **2016**, *103*, 117−123.
(32) Cotting, F.; Aoki, I. V. Smart Protection Provided by Epoxy Clear Coating Doped with Polystyrene Microcapsules Containing Silanol and Ce (III) Ions as Corrosion Inhibitors. *Surf. Coat. Technol.* **2016**, *303*, 310−318.
(33) Fan, W.; Li, W.; Zhang, Y.; Wang, W.; Zhang, X.; Song, L.; Liu, X. Cooperative Self-Healing Performance of Shape Memory Polyurethane and Alodine-Containing Microcapsules. *RSC Adv.* **2017**, *7*, 46778−46787.
(34) Wouters, M.; Craenmehr, E.; Tempelaars, K.; Fischer, H.; Stroeks, N.; van Zanten, J. Preparation and Properties of a Novel Remendable Coating Concept. *Prog. Org. Coat.* **2009**, *64*, 156−162.
(35) Luo, X.; Mather, P. T. Shape Memory Assisted Self-Healing Coating. *ACS Macro Lett.* **2013**, *2*, 152−156.
(36) Song, Y.-K.; Jo, Y.-H.; Lim, Y.-J.; Cho, S.-Y.; Yu, H.-C.; Ryu, B.-C.; Lee, S.-I.; Chung, C.-M. Sunlight-Induced Self-Healing of a Microcapsule-Type Protective Coating. *ACS Appl. Mater. Interfaces* **2013**, *5*, 1378−1384.
(37) Lutz, A.; van den Berg, O.; Van Damme, J.; Verheyen, K.; Bauters, E.; De Graeve, I.; Du Prez, F. E.; Terryn, H. A Shape-

DOI: 10.1021/acsami.8b06985
ACS Appl. Mater. Interfaces 2018, 10, 23369−23379

Recovery Polymer Coating for the Corrosion Protection of Metallic Surfaces. *ACS Appl. Mater. Interfaces* **2015**, *7*, 175−183.
(38) Fang, L.; Chen, J.; Zou, Y.; Chen, S.; Fang, T.; Lu, C.; Xu, Z. Self-Healing Epoxy Coatings via Focused Sunlight Based on Photothermal Effect. *Macromol. Mater. Eng.* **2017**, *302*, 1700059.
(39) Lendlein, A.; Kelch, S. Shape-Memory Polymers. *Angew. Chem., Int. Ed.* **2002**, *41*, 2034−2057.
(40) Zhao, Q.; Qi, H. J.; Xie, T. Recent Progress in Shape Memory Polymer: New Behavior, Enabling Materials, and Mechanistic Understanding. *Prog. Polym. Sci.* **2015**, *49-50*, 79−120.
(41) Fang, Z.; Zheng, N.; Zhao, Q.; Xie, T. Healable, Reconfigurable, Reprocessable Thermoset Shape Memory Polymer with Highly Tunable Topological Rearrangement Kinetics. *ACS Appl. Mater. Interfaces* **2017**, *9*, 22077−22082.
(42) Mata, D.; Scharnagl, N.; Lamaka, S. V.; Malheiro, E.; Maia, F.; Zheludkevich, M. L. Validating the Early Corrosion Sensing Functionality in Poly (ether imide) Coatings for Enhanced Protection of Magnesium Alloy AZ31. *Corros. Sci.* **2018**, DOI: 10.1016/j.corsci.2018.05.034.
(43) Galvão, T. L. P.; Sousa, I.; Wilhelm, M.; Carneiro, J.; Opršal, J.; Kukačková, H.; Špaček, V.; Maia, F.; Gomes, J. R. B.; Tedim, J.; Ferreira, M. G. S. Improving the Functionality and Performance of AA2024 Corrosion Sensing Coatings with Nanocontainers. *Chem. Eng. J.* **2018**, *341*, 526−538.
(44) Li, G.; Nettles, D. Thermomechanical Characterization of a Shape Memory Polymer Based Self-Repairing Syntactic Foam. *Polymer* **2010**, *51*, 755−762.
(45) Qian, H.; Xu, D.; Du, C.; Zhang, D.; Li, X.; Huang, L.; Deng, L.; Tu, Y.; Mol, J. M. C.; Terryn, H. A. Dual-Action Smart Coatings with a Self-Healing Superhydrophobic Surface and Anti-Corrosion Properties. *J. Mater. Chem. A* **2017**, *5*, 2355−2364.
(46) Xie, T.; Rousseau, I. A. Facile Tailoring of Thermal Transition Temperatures of Epoxy Shape Memory Polymers. *Polymer* **2009**, *50*, 1852−1856.
(47) Sinha, V. R.; Bansal, K.; Kaushik, R.; Kumria, R.; Trehan, A. Poly-ϵ-caprolactone Microspheres and Nanospheres: An Overview. *Int. J. Pharm.* **2004**, *278*, 1−23.
(48) Khoshroo, K.; Jafarzadeh Kashi, T. S.; Moztarzadeh, F.; Tahriri, M.; Jazayeri, H. E.; Tayebi, L. Development of 3D PCL Microsphere/TiO2 Nanotube Composite Scaffolds for Bone Tissue Engineering. *Mater. Sci. Eng., C* **2017**, *70*, 586−598.
(49) Wang, X.; Wang, Y.; Wei, K.; Zhao, N.; Zhang, S.; Chen, J. Drug Distribution within Poly(ε-caprolactone) Microspheres and in vitro Release. *J. Mater. Process. Technol.* **2009**, *209*, 348−354.
(50) Huang, X.; Li, N.; Wang, D.; Luo, Y.; Wu, Z.; Guo, Z.; Jin, Q.; Liu, Z.; Huang, Y.; Zhang, Y.; Wu, C. Quantitative Three-Dimensional Analysis of Poly (lactic-co-glycolic acid) Microsphere Using Hard X-ray Nano-Tomography Revealed Correlation Between Structural Parameters and Drug Burst Release. *J. Pharm. Biomed. Anal.* **2015**, *112*, 43−49.
(51) Balaskas, A. C.; Kartsonakis, I. A.; Tziveleka, L.-A.; Kordas, G. C. Improvement of Anti-corrosive Properties of Epoxy-Coated AA 2024-T3 with TiO2 Nanocontainers Loaded with 8-Hydroxyquinoline. *Prog. Org. Coat.* **2012**, *74*, 418−426.
(52) Lv, L.-P.; Landfester, K.; Crespy, D. Stimuli-Selective Delivery of Two Payloads from Dual Responsive Nanocontainers. *Chem. Mater.* **2014**, *26*, 3351−3353.
(53) Snihirova, D.; Lamaka, S. V.; Cardoso, M. M.; Condeço, J. A. D.; Ferreira, H. E. C. S.; de Fatima Montemor, M. pH-Sensitive Polymeric Particles with Increased Inhibitor-Loading Capacity as Smart Additives for Corrosion Protective Coatings for AA2024. *Electrochim. Acta* **2014**, *145*, 123−131.
(54) Maia, F.; Yasakau, K. A.; Carneiro, J.; Kallip, S.; Tedim, J.; Henriques, T.; Cabral, A.; Venâncio, J.; Zheludkevich, M. L.; Ferreira, M. G. S. Corrosion Protection of AA2024 by Sol-gel Coatings Modified With MBT-loaded Polyurea Microcapsules. *Chem. Eng. J.* **2016**, *283*, 1108−1117.
(55) Zhang, D.; Petersen, K. M.; Grunlan, M. A. Inorganic-Organic Shape Memory Polymer (SMP) Foams with Highly Tunable Properties. *ACS Appl. Mater. Interfaces* **2012**, *5*, 186−191.
(56) Snihirova, D.; Lamaka, S. V.; Taryba, M.; Salak, A. N.; Kallip, S.; Zheludkevich, M. L.; Ferreira, M. G. S.; Montemor, M. F. Hydroxyapatite Microparticles as Feedback-Active Reservoirs of Corrosion Inhibitors. *ACS Appl. Mater. Interfaces* **2010**, *2*, 3011−3022.
(57) Li, S.; Cui, Z.; Zhang, L.; He, B.; Li, J. The Effect of Sulfonated Polysulfone on the Compatibility and Structure of Polyethersulfone-Based Blend Membranes. *J. Membr. Sci.* **2016**, *513*, 1−11.
(58) Radhakrishnan, S.; Sonawane, N.; Siju, C. R. Epoxy Powder Coatings Containing Polyaniline for Enhanced Corrosion Protection. *Prog. Org. Coat.* **2009**, *64*, 383−386.
(59) Wang, L.; Deng, L.; Zhang, D.; Qian, H.; Du, C.; Li, X.; Mol, J. M. C.; Terryn, H. A. Shape Memory Composite (SMC) Self-Healing Coatings for Corrosion Protection. *Prog. Org. Coat.* **2016**, *97*, 261−268.
(60) Snihirova, D.; Liphardt, L.; Grundmeier, G.; Montemor, F. Electrochemical Study of the Corrosion Inhibition Ability of "Smart" Coatings Applied on AA2024. *J. Solid State Electrochem.* **2013**, *17*, 2183−2192.
(61) Kartsonakis, I. A.; Athanasopoulou, E.; Snihirova, D.; Martins, B.; Koklioti, M. A.; Montemor, M. F.; Kordas, G.; Charitidis, C. A. Multifunctional Epoxy Coatings Combining a Mixture of Traps and Inhibitor Loaded Nanocontainers for Corrosion Protection of AA2024-T3. *Corros. Sci.* **2014**, *85*, 147−159.
(62) Samadzadeh, M.; Boura, S. H.; Peikari, M.; Kasiriha, S. M.; Ashrafi, A. A Review on Self-Healing Coatings Based on Micro/Nanocapsules. *Prog. Org. Coat.* **2010**, *68*, 159−164.
(63) Balaskas, A. C.; Kartsonakis, I. A.; Snihirova, D.; Montemor, M. F.; Kordas, G. Improving the Corrosion Protection Properties of Organically Modified Silicate-Epoxy Coatings by Incorporation of Organic and Inorganic Inhibitors. *Prog. Org. Coat.* **2011**, *72*, 653−662.
(64) Snihirova, D.; Taryba, M.; Lamaka, S. V.; Montemor, M. F. Corrosion Inhibition Synergies on a Model Al-Cu-Mg Sample Studied by Localized Scanning Electrochemical Techniques. *Corros. Sci.* **2016**, *112*, 408−417.
(65) El-Nahass, M. M.; Farid, A. M.; Atta, A. A. Structural and Optical Properties of Tris(8-hydroxyquinoline) Aluminum (III) (Alq3) Thermal Evaporated Thin Films. *J. Alloys Compd.* **2010**, *507*, 112−119.
(66) Zheludkevich, M. L.; Yasakau, K. A.; Bastos, A. C.; Karavai, O. V.; Ferreira, M. G. S. On the Application of Electrochemical Impedance Spectroscopy to Study the Self-Healing Properties of Protective Coatings. *Electrochem. Commun.* **2007**, *9*, 2622−2628.
(67) González-García, Y.; Mol, J. M. C.; Muselle, T.; De Graeve, I.; Van Assche, G.; Scheltjens, G.; Van Mele, B.; Terryn, H. SECM Study of Defect Repair in Self-Healing Polymer Coatings on Metals. *Electrochem. Commun.* **2011**, *13*, 169−173.
(68) González-García, Y.; García, S. J.; Hughes, A. E.; Mol, J. M. C. A Combined Redox-Competition and Negative-Feedback SECM Study of Self-Healing Anticorrosive Coatings. *Electrochem. Commun.* **2011**, *13*, 1094−1097.
(69) Wang, W.; Xu, L.; Sun, H.; Li, X.; Zhao, S.; Zhang, W. Spatial Resolution Comparison of AC-SECM with SECM and Their Characterization of Self-Healing Performance of Hexamethylene Diisocyanate Trimer Microcapsule Coatings. *J. Mater. Chem. A* **2015**, *3*, 5599−5607.

DOI: 10.1021/acsami.8b06985
ACS Appl. Mater. Interfaces 2018, 10, 23369−23379